A novel effective nonlinear state observer based robust nonlinear sliding mode controller for a 6 kW Proton Exchange Membrane Fuel Cell Voltage Regulation.

Ali DALI[1], Samir ABDELMALEK*[2], Azzeddine BAKDI[3], Maamar BETTAYEB[4]

[1]Centre de Développement des Energies Renouvelables, CDER, BP 62 Route de l'Observatoire, Bouzaréah, Alger, 16340, Algérie.
Email: a.dali@cder.dz

*[2] Faculty of Technology, Department of Electrical Engineering, University of Medea, Algeria.
email: s.abdelmalek.dz@gmail.com

[3] Department of Mathematics, University of Oslo, 0851 Oslo, Norway.
Email: bkdaznsun@gmail.com

[4] Department of Electrical Engineering, University of Sharjah, United Arab Emirates, and Center of Excellence in Intelligent Engineering Systems (CEIES), King Abdulaziz University, Jeddah, KSA.
Email: maamar@sharjah.ac.ae

Abstract:

This paper presents an effective strategy for controlling an Interleaved DC/DC Boost Converter (IBC) that is employed for reducing the current fluctuations in a 6 kW Proton Exchange Membrane Fuel Cell (PEMFC). The proposed design incorporates a new nonlinear control law combined with a nonlinear state observer, it aims at enhancing the durability of the Fuel Cells (FCs) and extending their lifetime. In this regard, a Nonlinear State Observer (NSO) is designed to simultaneously estimate current and voltage signals of the Fuel Cell Source (FCS) and a Nonlinear Sliding Mode Controller (NSMC) is constructed based on these estimates. The proposed sensorless control design is advantageous in avoiding current and voltage sensors redundancy to maintain low cost and complexity levels. Accurate output voltage tracking performance, tracking stability, and dynamic errors for a PEMFC-IBC are considered during changes of the internal model parameters in addition to effects of measurement uncertainties. A third advantage of this design is robustness and external disturbance rejection under large load variations. For these objectives, the observer and the controller parameters are optimally tuned using a recent Metaheuristic Particle Swarm Optimization Algorithm (MPSOA) inspired by the swarm intelligence for improving the dynamic performance of the controlled system. Furthermore, stability and tracking analysis properties of the closed-loop overall system are proved through Lyapunov theory for dynamic operating conditions. Finally, numerical simulations of a typical 6 kW PEMFC system validate the effectiveness of the proposed scheme with comparisons to contemporary approaches across the different cases.

Keywords— Interleaved boost converter; Proton Exchange Membrane Fuel Cell; PSO algorithm; Nonlinear sliding mode control; PI controller; Nonlinear state observer.

Nomenclature

V_c	The output voltage	E	The controlled voltage source
V_{fc}	The Fuel Cell source voltage	E_{oc}	Open circuit voltage (V);
L	The inductance	N	Number of cells;
C	The capacitance	A_f	Tafel slope (V);
D_1, D_2	The duty cycles of each phase	i_0	Exchange current (A);
I_{L_1}, I_{L_2}	The inductors current	T_d	The response time (at 95% of the final value)
I_{fc}	The fuel cell current,	R_{ohm}	Internal resistance (Ω);
I_R	The resistor load current	i_{fc}	Fuel cell current (A);
I_c	The capacitor current	V_{fc}	Fuel cell voltage (V).
u	The average duty cycle	x_h	Percentage of hydrogen in the fuel (%)
z	Number of moving electrons (z = 2)	y_h	Percentage of oxygen in the oxidant (%)
E_n	Nernst voltage (V)	V_{cd}	Desired voltage
α	Charge transfer coefficient	I_{fc_d}	Desired fuel cell current
P_{H2}	Partial pressure of hydrogen inside the stack (atm)	k_1, k_2, k_3	Parameters of the proposed controller
P_{O2}	Partial pressure of oxygen inside the stack (atm)	$\boldsymbol{K_p}$, $\boldsymbol{K_i}$	Parameters of the PI controller
k	Boltzmann's constant (1.38×10−23 J/K)	$\boldsymbol{t}$	The iteration number;
h	Planck's constant (6.626×10−34 J s)	$\boldsymbol{j}$	The particle number;
ΔG	Activation energy barrier (J)	$\boldsymbol{p_j}$	The individual best solution of particle **j** at a given stage;
T	Temperature of operation (K)	$\boldsymbol{p_g}$	The global best solution;
Kc	Voltage constant at nominal condition of operation	$\boldsymbol{C_1}$, $\boldsymbol{C_2}$	The acceleration parameters;
P_{fuel}	Absolute supply pressure of fuel (atm)	$\boldsymbol{r_1}, \boldsymbol{r_2}$	Random numbers uniformly distributed
P_{air}	Absolute supply pressure of air (atm)		
V_{fuel}	Fuel flow rate (l/min)		
V_{air}	Air flow rate (l/min)		
P_{H_2O}	Partial pressure of water vapor (atm).		
w	Percentage of water vapor in the oxidant (%).		

Abbreviations

PEMFC	Proton-Exchange Membrane Fuel Cell
IBC	Interleaved Boost Converter
PI	Proportional Integral
PSO	Particle Swarm Optimization
IAE	Integral of Absolute Error
FCs	Fuel Cells
EVs	Electric Vehicles
MPC	Model Predictive Control
LTI	Linear Time-Invariant
NSO	Nonlinear State Observer

FCS	Fuel Cell Source
NSMC	Nonlinear Sliding Mode Controller
MPSOA	Metheuristic Particle Swarm Optimization Algorithm
PES	Power Energy Sources
RS	Renewable Sources
FLC	Fuzzy Logic Controller
MPPT	Maximum Power Point Trackers
SSAM	State-Space Average Modeling
MPSOA-NSMC	MPSOA -tuned Nonlinear Sliding Mode Controller
MPSOA-PIC	MPSOA -tuned Proportional Integral Controller

1- Introduction

Since the recent years, the global demand for energy is rising due to the huge amounts of energy consumption, and particularly in developing countries worldwide. Such demands are mainly fulfilled by various Power Energy Sources (PES) like fossil fuels, nuclear sources, thermal and renewable sources [1,10]. Energy generated from fossil-fuels sources (Oil and Petroleum Products, Hydrocarbon Gas Liquids, Natural Gas, Coal, Nuclear) leads to a severely negative impact on the environment such as the increase in carbon emissions which promotes atmospheric pollution and global warming. Therefore, the integration of Renewable Sources (RS) to power systems is becoming a key alternative to decrease the problems associated with the use of fossil fuels and to avoid greenhouse emissions and environmental damage [1-5,38].

Furthermore, FCs are also considered among the most growing and promising technologies for cleaner, efficient, and sustainable renewable power energy generation applications. Fuel cells are static devices [4,49] which convert the stored chemical energy Hydrogen and Oxygen in the reactant molecules to electrical energy directly through electrochemical reactions in the presence of catalysts. For this reason, the electrical efficiency of FCs is considerably highest compared to all traditional sources for generating electrical power [6], renewable energy power sources, besides, being eco-friendly [7,17,39].

In addition, PEMFC seems to be the most suitable FC technology which is widely used in several applications for automotive industry and especially electrified transportation industries [4, A], mobile applications [8], electrical vehicles [9, 16], hybrid tramways [B, C] and low power generation [11] as they offer many advantages such as low operating temperature, fast response to load changes, high power density, low corrosion, very low noise and environmental friendliness [1, 50]. Common types as well as pros and cons of fuel cell membranes are summarized in [15].

DC-DC boost converters are often used in different industrial power applications which have low output voltage like renewable energy power sources [12]. Generally, DC-DC converters are usually used to adapt the voltage and current levels between sources and loads while guarantying a low power loss in the power generation systems [13,14]. This converter is considered a necessary need and a crucial part of the FC power generation unit to effectively and efficiently control the power delivery. However, incorporating PEMFC dynamics with the classical DC-DC converter makes the voltage regulation task quite challenging [18]. In this context, the IBC presents a better solution which can be used to cope with the previous mentioned problems [19].The IBC is considered a good solution due to its advantages, such as high efficiency, ripple reduction, increasing the power level

and minimizing the current stress on the power switches [20]. So, IBCs offer additional benefits like reducing ripple currents in both input and output circuits which consequently reduces the stress on the devices in addition to their faster dynamics, higher efficiency, and low input voltage applications [21].

During recent years, several works on control strategies of DC/DC converters for PEMFC system were investigated. Authors in [22] proposed a nonlinear model predictive control strategy to enhance the efficiency and lifetime of PEMFC. A sliding mode observer was presented in [23] in order to estimate the state variables (nitrogen in the anode side and the relative humidity) in the channels for of PEMFC in automotive applications. A simple strategy based on a neural network tool for the regulation of the output voltage controlling an IBC associated to the PEMFC was adopted in [24]. Furthermore, an adaptive thermal control for PEMFC systems was developed in [25] for regulating the stack temperature, after that the obtained results were compared with the conventional PI controller. Also, authors in [26] presented a smart controller based on neural network for PEMFC sources. They proved that using neural optimal controller is better than PID controller, due to its automatic tuning capability and flexibility of the intelligent model-based controller. On the other hand, a second order sliding mode control scheme was developed by the authors for FC in vehicle. This control scheme can be used to deal with the slower dynamics of the FC [27].

In [28], an adaptive control technique was presented for DC/Dc converters. Similarly, a robust controller was also developed in [29], Takagi-Sugeno fuzzy controller was studied in [30, 31], and other controllers such as state feedback LQR control [32], sliding mode fuzzy PID controller [33], a robust adaptive neural network control [34], sliding mode control for PEM fuel cell applications [35], intelligent control [36], and Fuzzy Logic Controller (FLC) with Maximum Power Point Trackers (MPPT) were developed in [37]. However, among the presented control strategies which only aim at guaranteeing the system stability, the problem of optimal design of the nonlinear controllers in terms of robustness and optimal performance was not studied. Therefore, the objective of this work is to propose a novel control strategy, in which the controller and the observer parameters are then optimally determined against different robustness and performance criteria by using an effective tool which the so-called Metaheuristic Particle Swarm Optimization Algorithm (MPSOA). MPSOA showed superior performance in nonlinear and robust controllers in energy conversion applications [D, E], and it is developed in this work to optimize the novel control design.

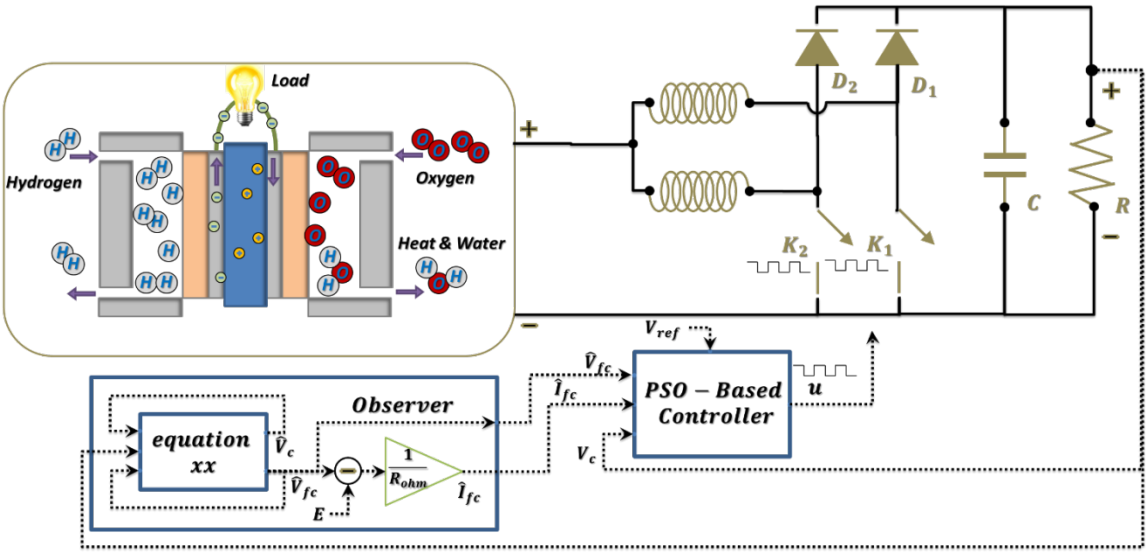

Fig. 1. Fuel Cell-Boost based IBC.

The major contributions of the present work are as follows: i) Using a new topology based on IBC rather than the traditional boost DC/DC converter to enhance and improve fuel cell output regulation, ii) A nonlinear state observer is presented for simultaneous estimation of the current and voltage signals of the Fuel Cell Source, iii) A new nonlinear control law combined with a nonlinear state observer is proposed for output voltage regulation under varying load conditions, (iv) Within the developed controller the need of additional sensors is not necessary due to state observer, which can provide the online information of current and voltage signals of the FCS, which will reduce the cost, (v) MPSOA-based optimal design determines the optimal parameters of the proposed controller and vi) Validation and comparison of the proposed controller with the MPSOA-based PI controller.

The remaining of this paper is organized as follows. Firstly, mathematical modelling of the physical DC-DC IBC system is presented in section 2. Section 3 then introduces a mathematical model for the entire system as shown in Fig. 1. The step-by-step design of the proposed control strategy is detailed in section 4. Section 5 describes parameter optimization using the MPSOA for both robust sliding nonlinear and conventional PI controllers. Different test results are summarized and discussed in section 6. The key aspects of this paper are presented in the last section including also some concluding remarks and suggestions for future work.

2- The Developed State Space Model of the IBC

Recently, IBCs are often used in many applications especially in power energy systems which provide low output voltage, like power electronic interfaces in renewable power energy sources such as photovoltaic and fuel cell systems.

The State-Space Average Modeling (SSAM) consists another alternative in which the converter is considered to operate in ON and OFF modes. A linear time-invariant model can be extracted for each mode and a unified average state-space model is obtained for the converter. The SSAM of the IBC is the same as the traditional boost DC-DC converter except that it contains two current inductors. The dynamics model of the IBC is given as [32]:

$$\begin{cases} L_1 \frac{dI_{L_1}}{dt} = V_{fc} - V_c(1 - D_1) \\ L_2 \frac{dI_{L_2}}{dt} = V_{fc} - V_c(1 - D_2) \\ C \frac{dV_c}{dt} = I_{L_1}(1 - D_1) + I_{L_2}(1 - D_2) - I_R \end{cases} \quad (1)$$

such that:

$$\begin{cases} I_{fc} = I_{L_1} + I_{L_2} \\ D_1 = D_2 = 1 - \mathrm{u} \\ L_1 = L_2 = L \end{cases} \quad (2)$$

where L and C represent respectively the inductance and the capacitance, $D_1$and D_2 are the duty cycles of each phase. I_{L_1} and I_{L_2} are the inductors' currents, I_{fc} is the FC current, $I_R = V_c/R$ is the resistor (R) load current and I_c is the capacitor current. Then, the SSAM of system (1) can be expressed as follows:

$$\begin{cases} \dot{I_{fc}} = \frac{2}{L} V_{fc} - \frac{2}{L} V_c u \\ \dot{V_c} = \frac{1}{C} I_{fc} u - \frac{1}{RC} V_c \end{cases} \quad (3)$$

where u is the average duty cycle.

Let us define the state vector $x = \left[I_{fc},\, V_c,\, \int V_c\, \right]^T$that contains the measurable output voltage (V_c) and the FC current (I_{fc}), the third state which is the integral of the measurable output voltage (V_c) is introduced in order to enhance and improve the robustness of the controller design. Then, a mathematical model of IBC with additional state variable is presented in Eq.(4):

$$\begin{cases} \dot{x}_1 = \frac{2}{L} V_{fc} - \frac{2}{L} x_2 u \\ \dot{x}_2 = \frac{1}{C} x_1 u - \frac{1}{RC} x_2 \\ \dot{x}_3 = x_2 \end{cases} \quad (4)$$

By manipulating the system equations (4), it is possible to write the ASSM as:

$$\dot{\mathcal{X}}(\mathrm{t}) = \begin{bmatrix} 0 & 0 & 0 \\ 0 & -\frac{1}{RC} & 0 \\ 0 & 1 & 0 \end{bmatrix} \begin{bmatrix} x_1 \\ x_2 \\ x_3 \end{bmatrix} + \begin{bmatrix} -\frac{2}{L} x_2 \\ -\frac{2}{C} x_1 \\ 0 \end{bmatrix} \mathrm{u}(\mathrm{t}) + \begin{bmatrix} \frac{2}{L} V_{fc} \\ 0 \\ 0 \end{bmatrix} \quad (5)$$

3- The Fuel Cell Mathematical Model

In this section, the mathematical model is derived for a fuel cell stack as a controlled voltage source in series with a constant resistance as displayed in Fig 2.

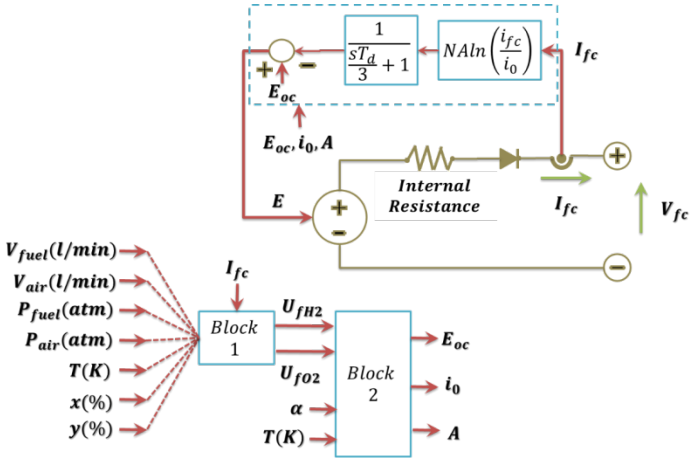

Fig. 2. fuel cell stack model.

The controlled voltage source (E) is expressed as [40-41]:

$$\begin{cases} E = E_{oc} - N\,A\,ln\left(\frac{i_{fc}}{i_0}\right)\frac{1}{s\frac{T_d}{3}+1} \\ V_{fc} = E - R_{ohm}i_{fc} \end{cases} \quad (6)$$

where,

E_{oc} : open circuit voltage (V);
N : number of cells;
A : Tafel slope (V);
i_0 : exchange current (A);
T_d : the settling time (at 95% of the final value) (sec);
R_{ohm} : internal resistance (Ω);
i_{fc} : fuel cell current (A);
V_{fc} : fuel cell voltage (V).

The open circuit voltage E_{oc}, the Tafel slope A and the exchange current i_0 are then expressed as follows [40]:

$$\begin{cases} E_{oc} = K_c E_n \\ i_0 = \frac{zFk(P_{H2}+P_{O2})}{Rh}\exp\left(\frac{-\Delta G}{RT}\right) \\ A = \frac{RT}{z\alpha F} \end{cases} \quad (7)$$

where

R = 8.3145 J/(mol K)
F = 96485 A s/mol
z = number of moving electrons (z = 2)
E_n = Nernst voltage (V)
α = charge transfer coefficient
P_{H2} = partial pressure of hydrogen inside the stack (atm)

P_{O2} = partial pressure of oxygen inside the stack (atm)
k = Boltzmann's constant (1.38×10−23 J/K)
h = Planck's constant (6.626×10−34 J s)
ΔG = activation energy barrier (J)
T = temperature of operation (K)
Kc = voltage constant at nominal condition of operation

The rates of conversion of Hydrogen (U_{fH2}) and Oxygen (U_{fO2}) are calculated in the block 1 as shown in Fig 2 as follows [40]:

$$\begin{cases} U_{fH2} = \frac{60000RTi_{fc}}{z\,F\,P_{fuel}V_{fuel}\,x\%} \\ U_{fO2} = \frac{60000RTi_{fc}}{z\,F\,P_{air}V_{air}\,y\%} \end{cases} \quad (8)$$

where

P_{fuel} = absolute supply pressure of fuel (atm)
P_{air} = absolute supply pressure of air (atm)
V_{fuel} = fuel flow rate (l/min)
V_{air} = air flow rate (l/min)
x = percentage of hydrogen in the fuel (%)
y = percentage of oxygen in the oxidant (%)

The partial pressures and the Nernst voltage are computed in the block 2 in Fig 2 as follows:

$$\begin{cases} P_{H2} = \left(1 - U_{fH2}\right)x\%P_{fuel} \\ P_{O2} = \left(1 - U_{fO2}\right)x\%P_{air} \\ P_{H_2O} = \left(w - 2y\%U_{fO2}\right)P_{air} \\ E_n = 1.229 - \frac{44.43}{zF}(T - 298) + \frac{RT}{zF}\ln\left(P_{H2}P_{O2}^{\frac{1}{2}}\right) \end{cases} \quad (9)$$

where

P_{H_2O} = partial pressure of water vapor (atm).
w = percentage of water vapor in the oxidant (%).

4- Design of the proposed NSMC

In the fuel cell power generations, the output and load power are time-varying and highly depend on operating conditions [46]. Therefore, the main goal of this section is to develop an appropriate switching approach so that it is possible to guarantee the optimal desired output against disturbances and model uncertainties. It was mentioned previously that the average state space LTI representation of the converter is quite sensitive to the changes in the reference output voltage, output load disturbances and the uncertainties in the parameters. Thus, a designed controller is then used

for satisfying a good trajectory tracking of the desired voltage (V_{ref}) by optimal compensation of the duty cycle (u) of the IBC switch.

4.1- NSMC theory

The Nonlinear Sliding Mode Control (NSMC) technique involves two steps: select the appropriate Sliding Surface (SS) for driving the system states to a predefined sliding manifold and for retaining them in the boundary layer region of the sliding manifold thereafter [42]. Then, the second step consists of designing a discontinuous state feedback capable of forcing the system to reach the state on the surface in finite time. The NSMC is considered as an efficient robust control technique for problems with nonlinear system subject to uncertainties and external disturbances. To date, NSMC is used in nonlinear power system stabilizers [43], power converters for pulse current charging [44], and DC–DC boost converters [45]. In addition, the dynamics structure of the NSMC system depends on the parameters of the switching surface and the choice of the latter is generally challenging.

4.2- Main results

The design procedure of the proposed NSMC scheme will be explained step by step in this section. Firstly, let us define the integral output voltage error, the output voltage error and the current tracking error as follows:

$$\begin{cases} e_1 = \int (V_{c_d} - V_c)dt \\ e_2 = V_{c_d} - V_c \\ e_3 = I_{fc_d} - I_{fc} \end{cases} \quad (10)$$

where V_{c_d} is the output reference voltage, e_2 is the tracking error between V_{c_d} and V_c, and e_3 is the current tracking error between I_{fc_d} and I_{fc}.

and,

$$I_{fc_d} = \frac{C}{u}\left(e_1 + \lambda_1 e_2 + \frac{1}{RC}\left(V_{c_d} - e_2\right) + \lambda_2\left(e_2 - e_{2_d}\right)\right) \quad (11)$$

From Eq.(10) and Eq.(11), the time derivative of e_1, e_2 and e_3 can be expressed by the following equations:

$$\begin{cases} \dot{e}_1 = e_2 \\ \dot{e}_2 = -\dot{x}_2 \\ \dot{e}_3 = \dot{I}_{fc_d} - \dot{x}_1 \end{cases} \text{ with } \dot{V}_{c_d} = 0 \quad (12)$$

***a) The existence condition of the NSMC*:**

The proposed sliding surface $S(t)$ is selected as follows:

$$S(e,t) = [e_1 \quad (e_2 + \lambda_1 e_1) \quad e_3] \quad (13)$$

where $\lambda_1$is positive constant.

Remark 1. The sliding surface Eq.(13) is selected with an integral term in order to deal with the time derivative of the error signal since this derivative will increase the noise signal ratio in a real time application.

Remark 2. The SS is selected based on the control objectives. Afterwards, the control signal is designed to ensure the existence of sliding mode condition. Thus, the system can converge to its SS in a finite time and remains on it.

b) Convergence condition:

After selecting the SS, the convergence condition ensures the system convergence to the selected SS. Thus, a positive-definite scalar function $V > 0$ must be found for the system state variable which is chosen using the following Lyapunov function:

$$V(x) = \frac{1}{2} S^2 \qquad (14)$$

The convergence condition is fulfilled if and only if:

$$V(x) < 0 \Rightarrow S(x)\dot{S^T}(x) < 0 \quad (15)$$

Stability of the proposed NSMC is principally analyzed through checking the existence and reaching conditions.

c) Calculation of the command law:

The controller structure contains two components, the first for an exact linearization and the second for stabilizing. The second one is very important in the NSMC technique, because it is used to eliminate the impression effects of the model and to reject disturbances. Thus, the control law has the following form:

$$u = u_{eq} + u_d \quad (16)$$

where the first term u_{eq} represents the equivalent control component, and the second term u_d corresponds to the discontinuous control. The objective of the curbing control is to force the system states to their intended SS values. Moreover, the curbing control eliminates the perturbation effect of the system uncertainties in practical applications. The equivalent control ensures that the system trajectory stays on the surface thereafter.

In this study, the discontinuous component is determined to achieve the attractiveness of the controlling variable to the SS and meet the following convergence condition:

$$S(x)\dot{S^T}(\mathrm{x}) < 0 \quad (17)$$

Using equations (5), (10)-(13) and (17):

$$S\dot{S^T} = e_1 e_2 + (e_2 + \lambda_1 e_1)\left(-\dot{V_c} + \lambda_1 e_2\right) + e_3 \dot{e_3} \quad (18)$$

Then,

$$S\dot{S^T} = e_1(e_2 - \lambda_1 e_1 + \lambda_1 e_1) + (e_2 + \lambda_1 e_1)\left(-\dot{V_c} + \lambda_1 e_2\right) + e_3 \dot{e_3} =$$

$$S\dot{S^T} = -\lambda_1 e_1^2 + (e_2 + \lambda_1 e_1)\left(e_1 - \dot{V_c} + \lambda_1 e_2\right) + e_3 \dot{e_3}$$

$$S\dot{S^T} = -\lambda_1 e_1^2 + (e_2 + \lambda_1 e_1)\left(e_1 - \left(\frac{1}{C} I_{fc} u - \frac{1}{RC} V_c\right) + \lambda_1 e_2\right) + e_3 \dot{e_3}$$

$$S\dot{S^T} = -\lambda_1 e_1^2 + (e_2 + \lambda_1 e_1)\left(e_1 + \lambda_1 e_2 - \left(\frac{1}{C} I_{fc} u - \frac{u}{C} I_{fc_d} + \frac{u}{C} I_{fc_d} - \frac{1}{RC} V_c\right)\right) + e_3 \dot{e_3}$$

$$S\dot{S^T} = -\lambda_1 e_1^2 + (e_2 + \lambda_1 e_1)\left(e_1 + \lambda_1 e_2 + \frac{u}{C} e_3 - \left(\frac{u}{C} I_{fc_d} - \frac{1}{RC} V_c\right)\right) + e_3 \dot{e_3} \quad (19)$$

with

$$I_{fc_d} = \frac{C}{u}\left(\frac{1}{RC}\left(V_{c_d} - e_2\right) + (\lambda_2 + 1)(e_2 + \lambda_1 e_1)\right) \quad (20)$$

Replacing the term (20) in the equation (19), yields to:

$$S\dot{S^T} = -\lambda_1 e_1^2 + (e_2 + \lambda_1 e_1)\left(-\lambda_2(e_2 + \lambda_1 e_1) + \frac{u}{C} e_3\right) + e_3 \dot{e_3}$$

$$S\dot{S^T} = -\lambda_1 e_1^2 - \lambda_2(e_2 + \lambda_1 e_1)^2 + e_3\left((e_2 + \lambda_1 e_1)\frac{u}{C} + \dot{I}_{fc_d} - \frac{2}{L} V_{fc} + \frac{2}{L} V_c u\right) \quad (21)$$

Then, the resulting control law (u) can be expressed by the following equation:

$$u = \frac{1}{\tau} + \left(-\dot{I}_{fc_d} + \frac{2}{L} V_{fc} - \lambda_3 e_3 - \eta sign(e_3)\right) \qquad (22)$$

with $\tau = 2\frac{V_c}{L} + \frac{e_2+\lambda_1 e_1}{C}$.

e) Stability study:

Using the same Lyapunov function in NSMC, it's clear that V is positive definite. Substituting (21) in (22), (22) leads to:

$$S\dot{S^T} = -\lambda_1 e_1^2 - \lambda_2(e_2 + \lambda_1 e_1)^2 - \lambda_3 e_3^2 - \eta|e_3| < 0 \quad (23)$$

which ensures that $V(x)$ is positive definite and consciously $\dot{V}(x)$ is negative definite. Thus, it can be concluded that the system is stable.

4.3- Nonlinear state observer design

In order to design a low-cost robust controller in the PEMFC-IBC system using NSMC approach, only one voltage sensor is employed for the output voltage V_c, the inductor current, fuel cell current, and voltage at different branches are then estimated by means of a recent proposed nonlinear state observer, where the following assumptions are considered:

A1. The fuel cell is approximated by the following equation:

$$V_{fc} = E - R_{ohm} I_{fc} \quad (24)$$

A2. Parameters variations in E and R_{ohm} are neglected.

Based on the assumptions (**A.1**) and (**A.2**), which yields to:

$$\dot{I}_{fc} = \frac{2}{L}V_{fc} - \frac{2}{L}V_c u \quad (25)$$

Then, we replace the I_{fc} and V_{fc} values and according to the above assumptions one can get:

$$\begin{cases} I_{fc} = \frac{1}{R_{ohm}}(E - V_{fc}) \\ V_{fc} = E - R_{ohm} I_{fc} \end{cases} \quad (26)$$

One can obtain the following equations:

$$\begin{cases} \dot{I}_{fc} = \frac{2}{L}V_{fc} - \frac{2}{L}V_c u \\ \dot{V}_c = \frac{1}{C}I_{fc} u - \frac{1}{RC}V_c \end{cases} \quad (27)$$

Then,

$$\begin{cases} \dot{V}_{fc} = -\frac{2R_{ohm}}{L}V_{fc} + \frac{2R_{ohm}}{L}V_c u \\ \dot{V}_c = \frac{1}{CR_{ohm}}(E - V_{fc})u - \frac{1}{RC}V_c \end{cases} \quad (28)$$

The structure of the proposed NSO for the system (28) is described as:

$$\begin{cases} \dot{\hat{V}}_{fc} = -\frac{2R_{ohm}}{L}\hat{V}_{fc} + \frac{2R_{ohm}}{L}\hat{V}_c u + L_1 u(\hat{V}_c - V_c) \\ \dot{\hat{V}}_c = \frac{1}{CR_{ohm}}(E - \hat{V}_{fc})u - \frac{1}{RC}\hat{V}_c + L_2(\hat{V}_c - V_c) \end{cases} \quad (29)$$

The state estimation errors (z_1 and z_2) are then defined as follows:

$$\begin{cases} z_1 = \hat{V}_{fc} - V_{fc} \\ z_2 = \hat{V}_c - V_c \end{cases} \quad (30)$$

By using Eqs.(28)-(30), the time derivative of z_1 and z_2 is determined as :

$$\begin{cases} \dot{z}_1 = -\frac{2R_{ohm}}{L}z_1 + \frac{2R_{ohm}}{L}uz_2 + L_1 uz_2 \\ \dot{z}_2 = -\frac{u}{CR_{ohm}}z_1 - \frac{1}{RC}z_2 + L_2 z_2 \end{cases} \quad (31)$$

Remark 4. The value of L_1 is selected as:

$$L_1 = -\frac{2R_{ohm}}{L} \qquad (32)$$

Remark 5. We take that:

$$\begin{cases} h_1 = \frac{2R_{ohm}}{L} \\ h_2 = \frac{-u}{CR_{ohm}} \\ h_3 = -\frac{1}{RC} + L_2 \end{cases} \qquad (33)$$

Based on the previous remarks (4)-(5), $\dot{z}_1$ and $\dot{z}_2$ are simplified as:

$$\begin{cases} \dot{z}_1 = -h_1 z_1 \\ \dot{z}_2 = h_2 z_1 + h_3 z_2 \end{cases} \qquad (34)$$

In order to study the stability of the proposed observer structure, the following Lyapunov function is proposed as follows:

$$V = \frac{1}{2} z_1^2 + \frac{1}{2}\left(z_2 + \frac{h_2}{h_1 + h_3} z_1\right)^2 \qquad (35)$$

The derivative of the Eq. (35) with respect to time is:

$$\dot{V} = -h_1 z_1^2 + \left(z_2 + \frac{h_2}{h_1 + h_3} z_1\right)\left(h_2 z_1 + h_3 z_2 - \frac{h_1 h_2}{h_1 + h_3} z_1\right)$$

$$\dot{V} = -h_1 z_1^2 + \left(z_2 + \frac{h_2 h_3}{1 - h_1 h_3} z_1\right)\left(\frac{h_2 h_3}{1 - h_1 h_3} z_1 + h_3 z_2\right)$$

$$\dot{V} = -h_1 z_1^2 + h_3 \left(z_2 + \frac{h_2 h_3}{1 - h_1 h_3} z_1\right)^2 \qquad (36)$$

In order to satisfy $\dot{V} < 0$, it is necessary in the case study to choose $h_3 \ll 0$, this means $L_2 \ll \frac{1}{RC}$.

Remark 6. In this case the proposed control law (u) will be replaced by ρu, ρ is a factor which includes all perturbations and uncertainties effects of the global system, which is selected by optimization as $\rho = 0.975$.

Remark 7. where k_1, k_2 and k_3 are positive constants whose values can be selected in the following section.

The parameters k_1, k_2, and k_3 of the proposed controller of Eq. (23) are heuristically determined using PSO technique, which is the object of section 6.

5- PI Controller Design

The second controller of a Proportional Integral (PI) controller which is also used to ensure the optimal regulation of the IBC converter's output, which has the following structure:

$$u(t) = 1 - U_{pi} \qquad (37)$$

with

$$U_{pi} = K_p\left(V_{cref} - V_{fc}\right) + K_i \int \left(V_{cref} - V_{fc}\right) dt \qquad (38)$$

The parameters K_p and K_i of the PI controller of Eq. (38) are heuristically tuned using MPSOA, which is the object of the following section.

6- MPSOA-based Controllers' Parameters

Metaheuristic Particle Swarm Optimization Algorithm (MPSOA) is a stochastic optimization technique. Since its first introduction in 1995 by [48], it was widely adopted for optimization problems in various engineering fields, and many variants of this algorithm were then proposed. MPSOA is known for its speed and computational efficiency for searching the global optimal solution is a manner that simulates birds searching for food or movement of fishes' shoal. This swarm-intelligent search algorithm is based on a swarm of N_p particles which represent some candidate solutions. These particles have changing positions in the search space of the optimization problem and they proceed towards the optimal solution after successive iterations. The expected final result is the convergence of the particle swarm towards the global best position in the search space, thus, the movement of each particle has influence on its historical best position as well as the optimal solution. A particle i of the swarm is defined by its actual position vector $(\boldsymbol{z}_i)$, movement velocity vector $(\boldsymbol{v}_i)$, and best position $\left(\boldsymbol{p}_{best,i}\right)$ in all previous iterations, and the global best position $(\boldsymbol{g}_{best})$ among all particles during a successive iteration.

The i^{th} particle moves towards its new position at the $(k+1)^{th}$ iteration as followas [47]:

$$\boldsymbol{z}_i^{k+1} = \boldsymbol{z}_i^k + \boldsymbol{v}_i^{k+1} \quad \text{for} \quad i = 1,2,\cdots,N_p \tag{39}$$

and the update iteration velocity at this iteration is [47]:

$$\boldsymbol{v}_i^{k+1} = \omega \boldsymbol{v}_i^k + c_1 r_1\left(\boldsymbol{p}_{best,i} - \boldsymbol{z}_i^k\right) + c_2 r_2\left(\boldsymbol{g}_{best} - \boldsymbol{z}_i^k\right) \quad \text{for} \quad i = 1,2,\cdots,N_p \tag{40}$$

where ω is the inertia weight parameter that affects the movement propagation, and the acceleration parameters c_1 and c_2 are respectively the cognitive coefficient of the individual particles and the social coefficient of all the particles, while r_1 and r_2 are random variables between 0 and 1, these control the influence of social and individual values.

The MPSOA has a significant advantage since it does not use Gradient Descent method and it can be applied to a nonlinear indifferentiable problem. In a nonlinear and uncertain framework, the goal of this work is to determine the optimal parameters of each controller in order to attain the best referenced tracking.

The objective function is therefore selected here as the Integral Absolute-value of the Error (IAE). The instantaneous error reflects input-output error between the reference and actual values achieved by the system according to its model Eq. (41), the minimum value of each iteration dictates the adaptive value. The main objective function is given as follows:

$$IAE = \int_0^{t_f} \left|V_{cref}(t) - V_c(t)\right| dt$$

$$subject\ to: \begin{cases} K_{p_{min}} < K_p < K_{p_{max}} \\ K_{d_{min}} < K_d < K_{d_{max}} \\ k_{1_{min}} < k_1 < k_{1_{max}} \\ k_{2_{min}} < k_2 < k_{2_{max}} \\ k_{3_{min}} < k_3 < k_{3_{max}} \\ k_{4_{min}} < k_4 < k_{4_{max}} \\ L_{1_{min}} < L_1 < L_{1_{max}} \\ L_{2_{min}} < L_2 < L_{2_{max}} \end{cases} \tag{41}$$

where t_f is the end time of simulation.

Function in Eq. (41) is considered also as the performance index of each controller design (the proposed design and the PSO-based PI). The different steps used in PSO-based tuning of the proposed and the PI controllers are illustrated in Fig. 3.

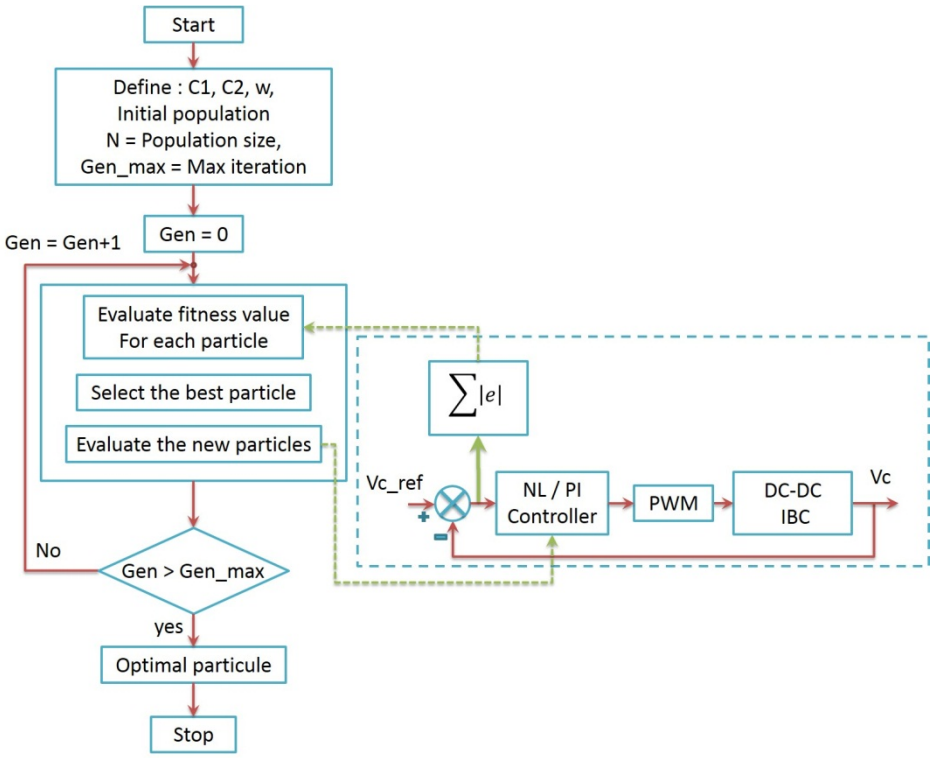

Fig. 3 Block diagram of the proposed PSO-based control design.

7- Results and discussion

In this section, the proposed controller for the DC-DC interleaved boost converter is designed using a set of parameters for IBC and fuel cell are respectively listed in Table I and Table II.

Table I. Parameters of a DC-DC interleaved boost converter**.**

Parameter	Value
L	$5000\ \mu H$
C	$1000\ \mu F$
R_L	$0.2\ \Omega$
R	$15\ \Omega$

Table II. Fuel cell parameters (A 6kW-48V fuel cell stack)

Parameter	Value	Components name
FC_Eoc	65	Voltage at 0 A (V)
FC_V1	63	Nominal operating Current (A)
FC_Inom	133.3	Voltage at 1 A (V)

FC_Vnom	45	Nominal operating Voltage (V)
FC_Imax	225	Maximum operating Current (A)
FC_Vmin	37	Minimum operating Voltage (V)
FC_N	65	Number of cells in series
FC_Tnom	65	Operating temperature (°C)
FC_Nnom	55	Nominal stack efficiency (%)
FC_Vair	300	Nominal air flow rate (L/min)
FC_Pfuel	1.5	Nominal supply pressure Fuel (bar)
FC_Pair	1	Nominal supply pressure Air (bar)
FC_Ph2	99.95	Nominal composition of H2 (%)
FC_Po2	21	Nominal composition of O2 (%)
FC_Ph2o	1	Nominal composition of H2O (Air) (%)
Rohm	0.8787	
E	57.36	

Remark 8. In order to approximate real system function, we considered that the inductance has an internal resistance of R_L = 0.2 Ω. This later will appear as an uncertainty error, which will also be used to verify the robustness of the proposed approach.

The MPSOA parameters for each controller design and the search range are listed in Table III and IV, respectively.

Table III. Optimum parameters used for MPSOA-based tuning of the proposed and PI controllers

MPSOA parameters	Value	
	MPSOA- PIC	MPSOA-NSMC
C_1	1	1
C_2	3	3
w	0.8	0.8
Population size	100	100
Maximum iteration	20	20

Table IV. Search range of the controller parameters

Controller parameters	Search range	
	Min	Max
k_1	100	1000
k_2	100	1000
k_3	1000	2000
K_p	0	10
K_i	0	10

The gains k_1 , k_2, k_3, and k_4 values of both controllers, in addition to K_p and K_i gains of the PI controller are heuristically tuned by solving the optimization problem in Eq.(28), this procedure is shown in Fig. 3. Then, the obtained final gains are summarized in Table V.

Table V. The optimal controllers' and observer parameters.

MPSOA- PIC	$K_p = 0.015, \quad K_i = 3.410$
MPSOA-NSMC	$k_1 = 253, \ k_2 = 217, \ k_3 = 1646, \ k_4 = 945$
MPSOA-NSO	$L_1 = -351.48 \quad L_2 = -4\ 10^4$

In this section, to validate the effectiveness and robustness of the proposed innovative control scheme for the IBC, two different numerical tests were performed under the deferent output reference voltage and then under the load disturbances. The overall performance of the PEMFC-fed IBC is verified for both MPSOA-PI and MPSOA-NSM controllers through the dynamic output characteristics and will be discussed hereafter.

A Simulink platform was developed to simulate the system as depicted in Fig. 4.

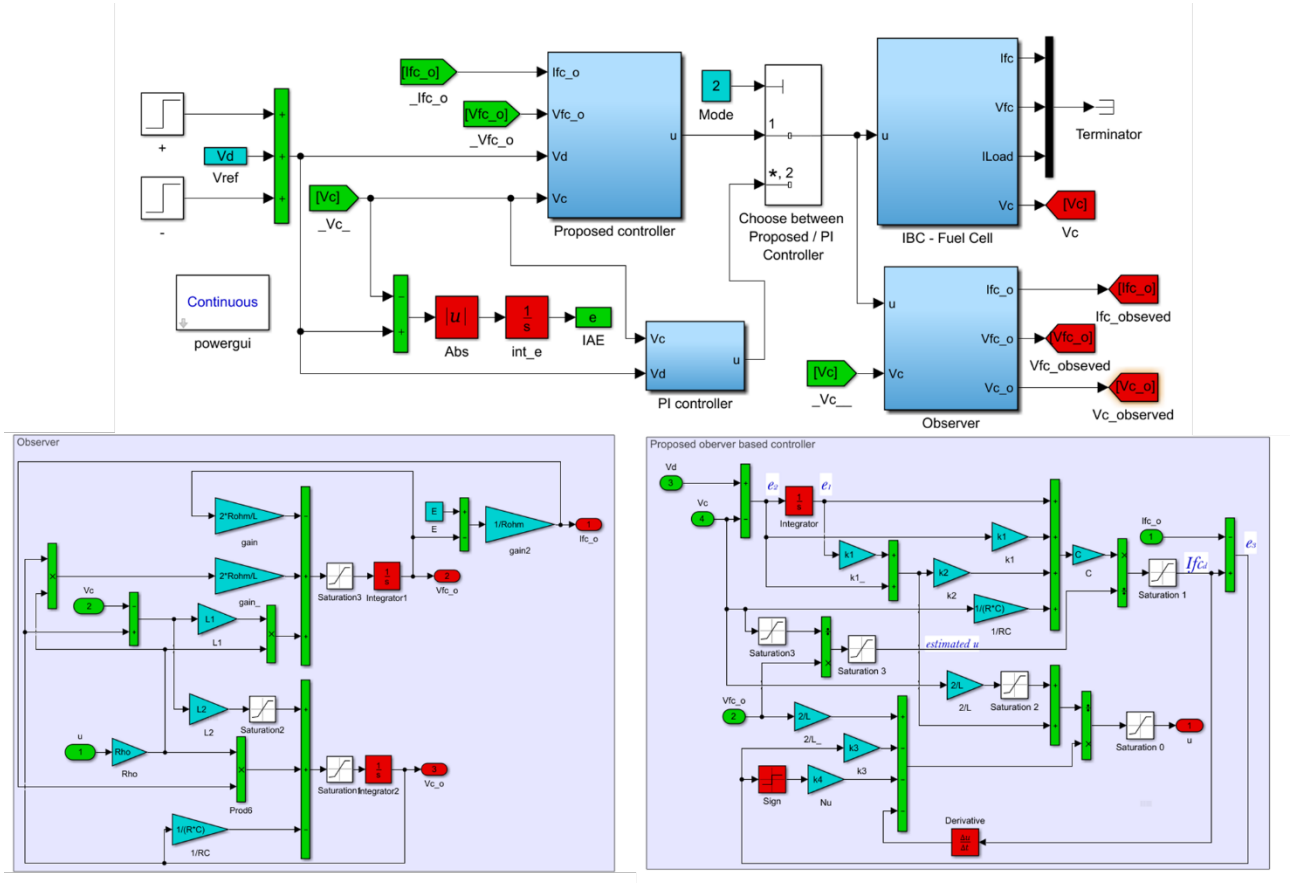

Fig. 4 Matlab/Simulink Model of the proposed system.

7-1. Disturbance in Input Voltage

In order to test the robustness of the proposed controller against variation of reference output voltage though abrupt step changes:

$$V_{cref} = \begin{cases} V_0 = 70\ V & 0s \le t \le 0.1s \\ 90\% * V_0 & 0.1s \le t \le 0.2s \\ 100\% * V_0 & 0.2s \le t \le 0.3s \end{cases} \qquad (29)$$

applied for short intervals to the IBC input voltage. The obtained results are depicted in Fig. 5. It is observed from Fig. 5 that the proposed controller (MPSOA-NSMC) can perfectly regulate the output voltage of the IBC. It can be seen also from Fig. 5 that MPSOA-NSMC settles to the final value within a shorter Rising time as listed in the Table VI. The MPSOA-NSMC ensures a smaller Overshoot and less ripples compared to the MPSOA-PIC as summarized in the Table V.

Table VI. Rise time results for the PEMFC-fed IBC system for both optimized controllers

Time (s)	[0.0 0.1]	[0.1 0.2]	[0.2 0.3]
MPSOA- PIC	0.0081	0.0037	0.0065
MPSOA-NSMC	**0.0027**	**0.0036**	**0.0056**

Table V. Overshoot performance of both controllers

Time (s)	[0.0 0.1]	[0.1 0.2]	[0.2 0.3]
MPSOA- PIC	9.30	2.32	2.91 (first) – 2.64 (second)
MPSOA-NSMC	**0.66**	**1.94**	**1.99 (first) –0.11(second)**

Furthermore, for statistic comparison, an IAE criterion is used for both methods and the corresponding results are summarized in the Table VII. The results confirm that the proposed controller (MPSOA-NSMC) leads to a more reliable performance for accurate and fast-settling output regulation of the IBC's load voltage than the MPSOA-PIC in term of the IAE criterion.

Table VII. Performance index of the proposed and PSO- PI controllers.

$\boldsymbol{IAE = \int_0^\infty \lvert e(t) \rvert \, dt}$			
Time (s)	[0.0 0.1]	[0.1 0.2]	[0.2 0.3]
MPSOA- PIC	0.0843	0.0447	0.1149
MPSOA-NSMC	**0.0271**	**0.0516**	**0.0916**

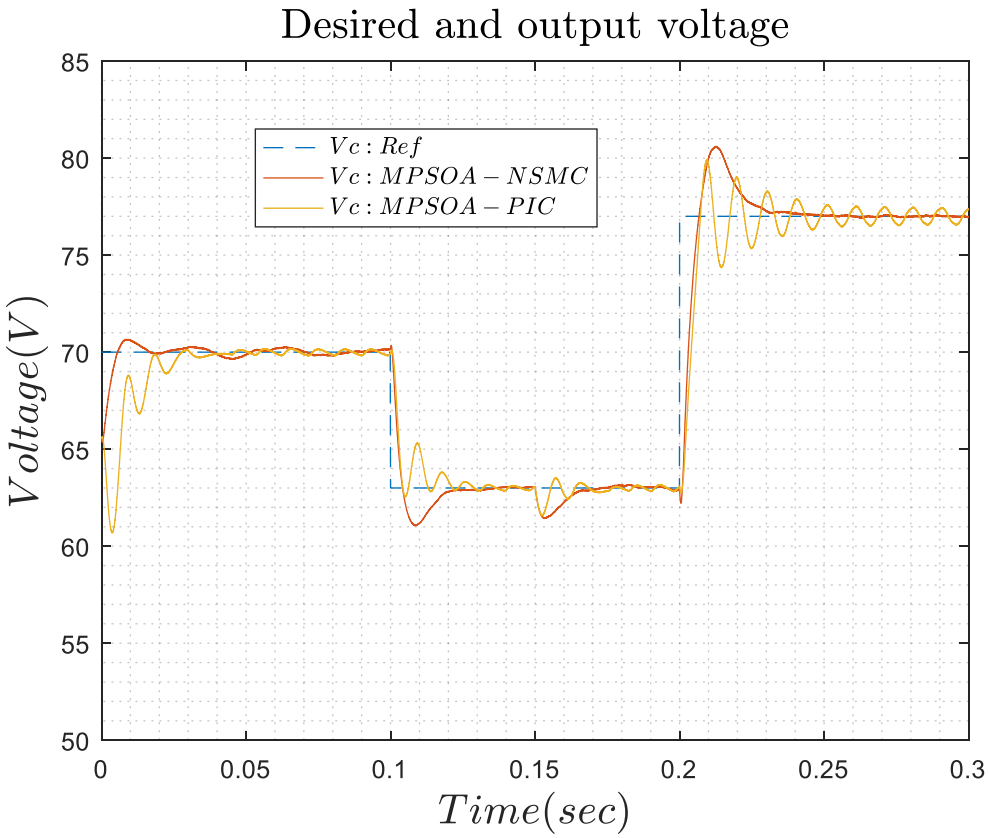

Fig. 5. Simulations under disturbance in output voltage.

The corresponding load, fuel cell currents and fuel cell voltage are respectively shown in Fig. 6. It can be seen from these figures that the proposed MPSOA-NSMC controller provides the smaller ripples in both of the output voltage and fuel cell currents as well as fuel cell voltage under variation of the input voltage. In addition, it can be concluded that, the proposed controller MPSOA-NSMC shows a stronger robustness to the input voltage disturbances compared to its MPSOA-PIC counterpart.

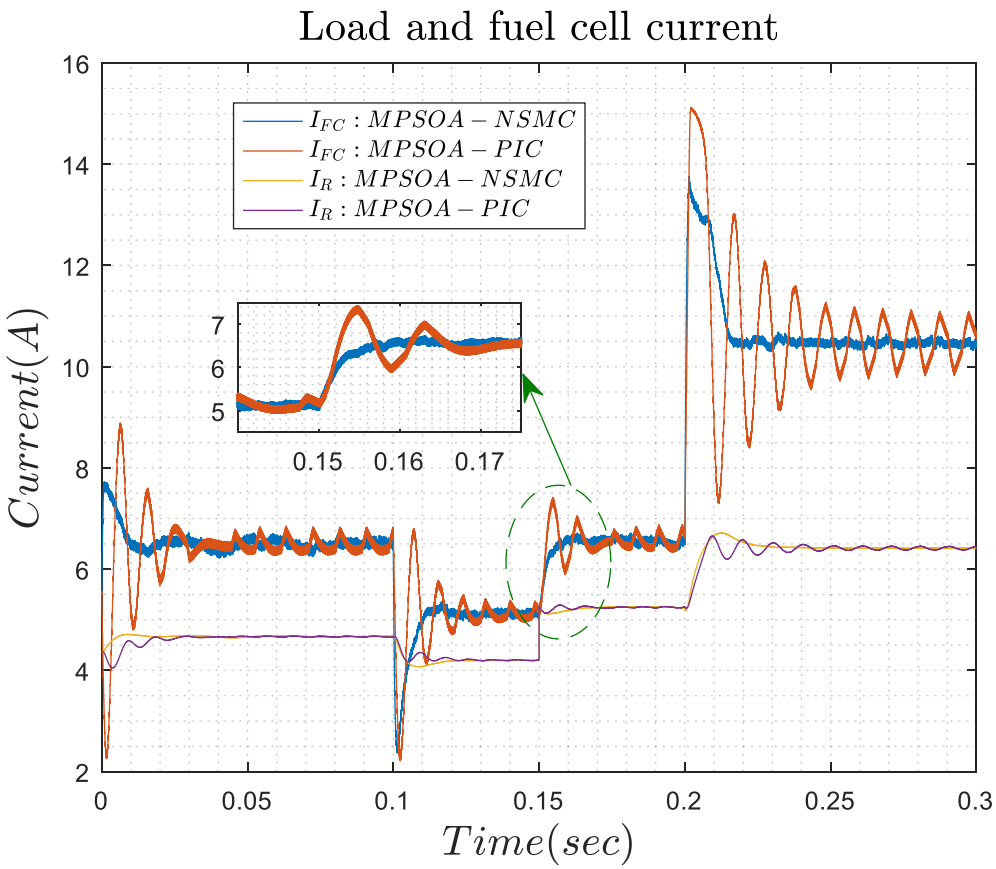

Fig. 6. Fuel cell and load currents response to output voltage variation.

7-2. Disturbance in Output Load Resistance:

In order to test the robustness of the proposed controller for the IBC under load disturbances and variations, the load variation of -20% is introduced at t=0.05s. The corresponding results are compared and pictured in Figs. 5–7.

Figs. 5–7 demonstrate the response of the regulated output voltage of the IBC, Fuel cell and load currents and the fuel cell voltage for 20% variation in load at t = 0.05 s. From these figures, it is clear that the closed loop system using the MPSOA-NSMC can withstand load variations and the output voltage has a smaller overshoot (0.43 instead of 9.30 for PI controller), (1.78 instead of 2.30 for PI controller) when is subjected to increase or decrease in load current and reaches the reference voltage within a settling time of 0.01 s. More detailed results are listed Table VIII.

Table VIII. Overshoot

Time (s)	[0.0 0.1]	[0.1 0.2]	[0.2 0.3]
MPSOA- PIC	9.30	2.32	2.91 (first) – 2.64 (second)
MPSOA-NSMC	**0.43**	**1.78**	**1.92 (first) –0.21 (second)**

We evaluated also the dynamic response of the system using the settling time defined in our case as the time required for the response to rise from initial value and reach 90% of its final value and remain withing an error band of $\pm$10% of the final value, these results are listed in table IX.

Table IX. Settling time

Time (s)	[0.1 0.2]	[0.2 0.3]
MPSOA- PIC	0.0188	0.0259
MPSOA-NSMC	**0.0159**	**0.0220**

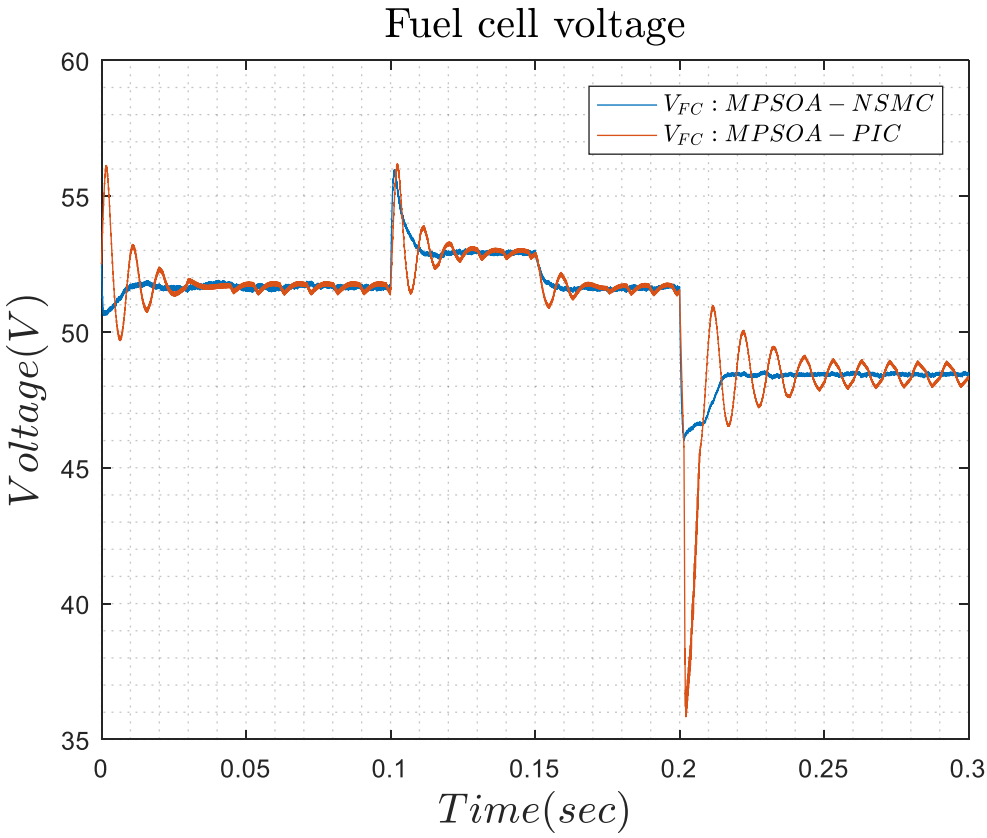

Fig. 7. Fuel Cell voltage under input voltage variation.

Fig. 8 and 9 represent respectively the voltage and load current responses, both real and observed signals are depicted for comparisons. These figures show that the proposed observer (MPSOA-NSO) has the ability to ensure simultaneous state tracking for both voltage and current states of the real fuel cell system with high accuracy regardless of load variations.

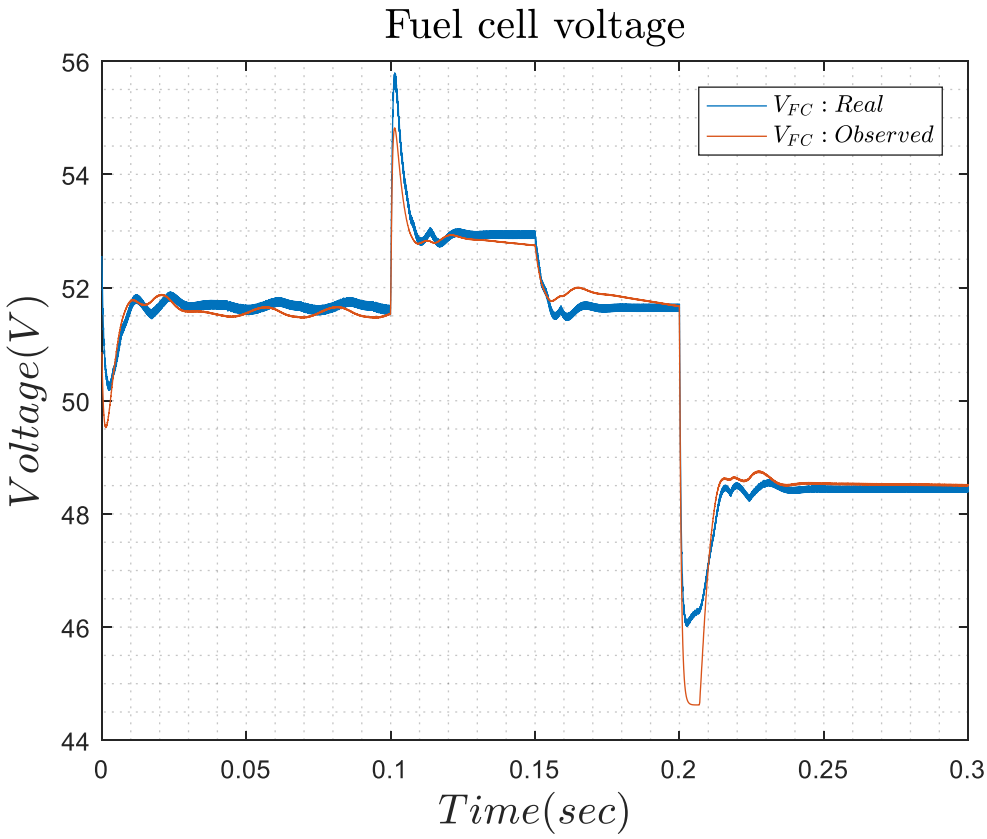

Fig. 8. The real and observed Fuel cell voltage.

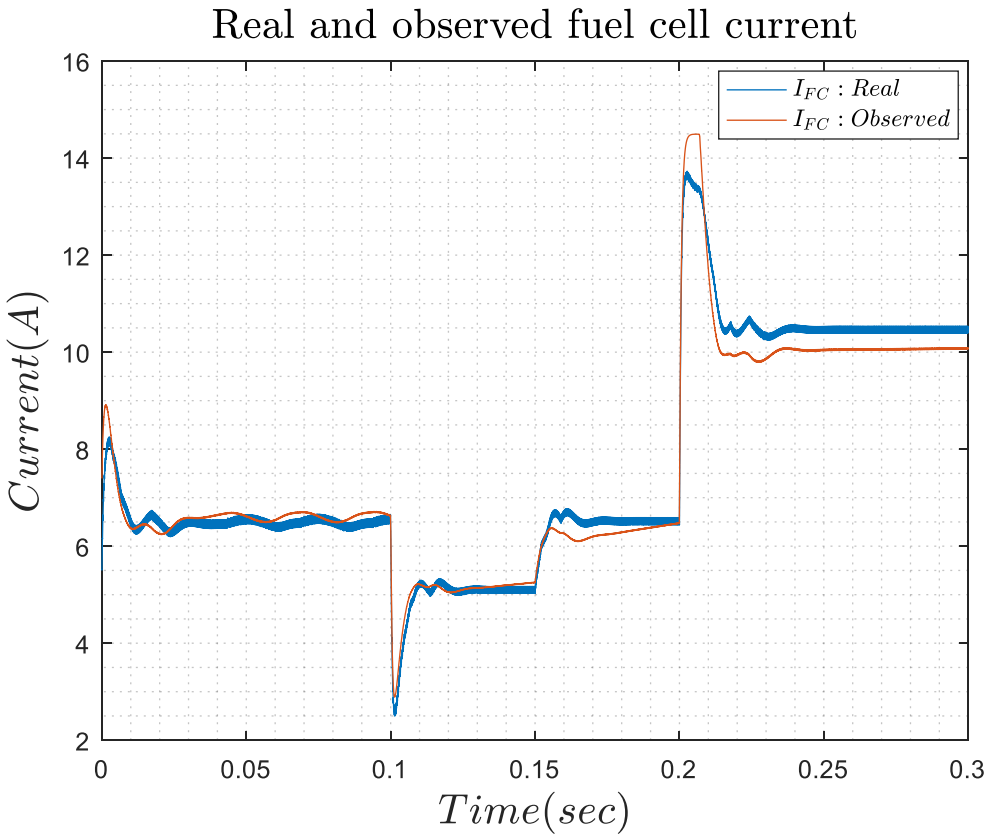

Fig. 10. The real and observed Fuel cell current.

As a consequent, in the presence of such parameter uncertainties and load variations, one can see that the proposed controller is capable to achieve significant improvements in the voltage regulation performance and this verifies the robustness of the proposed controller. It can be concluded from the comparison of those results that the proposed controller is able to effectively track the variations in the reference voltage of the PEMFC-fed IBC, and shows strong robustness to the load disturbance and input voltage variations.

8. Conclusion

This work considered the important problem of the output voltage regulation of a PEMFC-fed DC-DC interleaved boost converter in presence of model uncertainties and abrupt large variations in the output voltage as well as the load. A complete representative model is first developed for the fuel cell and the DC-DC IBC system. A nonlinear controller is developed based on state observation and sliding mode control. The observer-based system is advantageous over traditional sensors for its reduced cost and system complexity in addition to its robustness to hardware failures and automatic fault detection capability. The control problem was formulated using Lyapunov stability theorem and the design was optimized using MPSOA to ensure the nonlinear controller is further robust and effective. It was illustrated that the proposed controller is capable to ensure smooth regulation of the IBC output voltage under extreme cases. Robustness was verified through the tracking error against uncertainties in the parameters of the model and sudden variations. The integrated PSO optimized NSM controller and NSO together not only ensure high performance of the PEMFC-fed IBC for fast and smooth tracking, but also demonstrate very high robustness to setpoint changes,

parameter uncertainties, and load variations. This superiority is verified through simulations and comparisons of results across various scenarios reflect the improved performance achieved by the MPSOA-NSMC compared to the MPSOA-PIC in terms of transient behavior and minimum ripples during steady state. Those obtained results promote potential applications for the presented design in practice.

Conflict of interest

The authors declare that they have no known competing financial interests or personal relationships that could have appeared to influence the work reported in this paper.

References

[1]. P. T. Bankupalli, S. Ghosh, L. Kumar, S. Samanta. Fractional order modeling and two loop control of PEM fuel cell for voltage regulation considering both source and load perturbations. International Journal of Hydrogen Energy 2018, 43(12): 6294-6309.

[2]. M. Grötsch, M. Mangold, A. Kienle. Analysis of the coupling behavior of PEM fuel cells and DC-DC converters. Energies 2009, 2(1): 71-96.

[3]. J. Solé, A. García-Olivares, A. Turiel, J. Ballabrera-Poy. Renewable transitions and the net energy from oil liquids: A scenarios study. Renewable Energy 2018, 116: 258-271.

[4]. V. Das, S. Padmanaban, K. Venkitusamy, R. Selvamuthukumaran, F. Blaabjerg, P. Siano. Recent advances and challenges of fuel cell based power system architectures and control–A review. Renewable and Sustainable Energy Reviews 2017, 73: 10-18. :

[5]. S. Bendoukha, S. Abdelmalek, S. Abdelmalek. A new combined actuator fault estimation and accommodation for linear parameter varying system subject to simultaneous and multiple faults: an LMIs approach. Soft Computing 2018, 1-14.

[6]. E. Dijoux, N.Y. Steiner, M. Benne, M.C. Péra, B.G. Pérez. A review of fault tolerant control strategies applied to proton exchange membrane fuel cell systems. Journal of Power Sources 2017, 359: 119-133.

[7]. R. Patel, D. Deb. Parametrized control-oriented mathematical model and adaptive backstepping control of a single chamber single population microbial fuel cell. Journal of Power Sources 2018, 396: 599-605.

[8]. J. Luna, E. Usai, A. Husar, M. Serra. Enhancing the efficiency and lifetime of a proton exchange membrane fuel cell using nonlinear model-predictive control with nonlinear observation. IEEE transactions on industrial electronics 2017, 64(8): 6649-6659.

[9]. Q. Li, W. Chen, Z. Liu, A. Guo, S. Liu. Control of proton exchange membrane fuel cell system breathing based on maximum net power control strategy. Journal of Power Sources 2013, 241: 212-218.

[10]. M. M. Morato, D. J. Regner, P. R. Mendes, J.E. Normey-Rico, C. Bordons. Fault Analysis, Detection and Estimation for a Microgrid via H2/H∞ LPV Observers. International Journal of Electrical Power & Energy Systems 2019, 105: 823-845.

[11]. C. Qin, J. Wang, D. Yang, B. Li, C. Zhang. Proton exchange membrane fuel cell reversal: a review. Catalysts 2016, 6(12): 197.

[12]. W. R. W. Daud, R.E. Rosli, E.H. Majlan, S.A.A. Hamid, R. Mohamed, T. Husaini. PEM fuel cell system control: A review. Renewable Energy 2017, 113, 620-638.

[13]. A. Dali, S. Abdelmalek, M. Bettayeb. A New Combined Observer-State Feedback (COSF) Controller of PWM Buck Converter. In 2018 International Conference on Electrical Sciences and Technologies in Maghreb (CISTEM) 2018, 1-6.

[14]. A. Dali, S. Abdelmalek, M. Bettayeb. An Improved Observer-based Integral State Feedback (OISF) Control Strategy of Flyback Converter for Photovoltaic Systems. In 2018 International Conference on Electrical Sciences and Technologies in Maghreb (CISTEM) 2018, 1-6.

[15]. E. Ogungbemi, O. Ijaodola, F.N. Khatib, T. Wilberforce, Z. El Hassan, J. Thompson, M. Ramadan, A.G. Olabi. Fuel cell membranes – pros and cons, Energy 2019, 172: 155-172.

[16]. K. J. Reddy, S. Natarajan. Energy sources and multi-input DC-DC converters used in hybrid electric vehicle applications–A review. International Journal of Hydrogen Energy 2018, 43(36), 17387-17408.

[17]. M. İnci, Ö. Türksoy. Review of fuel cells to grid interface: Configurations, technical challenges and trends. Journal of Cleaner Production 2019, 213: 1353-1370.
[18]. S. Y. Choe, J. G. Lee, J. W. Ahn, S. H. Baek. Integrated modeling and control of a PEM fuel cell power system with a PWM DC/DC converter. Journal of Power Sources 2007, 164(2): 614-623.
[19]. C. M. Wang, C. H. Lin, S. Y. Hsu, C. M. Lu, J. C. Li. Analysis, design and performance of a zero-current-switching pulse-width-modulation interleaved boost dc/dc converter. IET Power Electronics 2014, 7(9): 2437-2445.
[20]. S. Somkun, C. Sirisamphanwong, S. Sukchai. A DSP-based interleaved boost DC–DC converter for fuel cell applications. international journal of hydrogen energy 2015, 40(19): 6391-6404.
[21]. J. A. Rahavi, T. Kanagapriya,R. Seyezhai. Design and analysis of interleaved boost converter for renewable energy source. In 2012 International Conference on Computing, Electronics and Electrical Technologies (ICCEET) 2012, 447-451.
[22]. J. Luna, E. Usai, A. Husar, M. Serra. Enhancing the efficiency and lifetime of a proton exchange membrane fuel cell using nonlinear model-predictive control with nonlinear observation. IEEE transactions on industrial electronics 2017, 64(8): 6649-6659.
[23]. M. Piffard, M. Gerard, R. Da Fonseca, P. Massioni, E. Bideaux. Sliding mode observer for proton exchange membrane fuel cell: automotive application. Journal of Power Sources 2018, 388: 71-77.
[24]. E. Barhoumi, I. Ben Belgacem, A. Khiareddine, M. Zghaibeh, I. Tlili. A Neural Network-Based Four Phases Interleaved Boost Converter for Fuel Cell System Applications. Energies 2018, 11(12): 3423.
[25]. L. Huang, Z. Chen, Liu, M Becherif. Adaptive thermal control for PEMFC systems with guaranteed performance. International Journal of Hydrogen Energy 2018, 43(25): 11550-11558.
[26]. P.E. Almeida, M.G. Simoes. Neural optimal control of PEM-fuel cells with parametric CMAC networks. In 38th IAS Annual Meeting on Conference Record of the Industry Applications Conference 2003, 2: 723-730.
[27]. L. C. Iwan, R. F. Stengel. The application of neural networks to fuel processors for fuel-cell vehicles. IEEE Transactions on Vehicular Technology 2001, 50(1): 125-143.
[28]. J. T. Su, D.M. Liu, C. W. Liu, C.W. Hung. An adaptive control method for two-phase DC/DC converter. International Conference on Power Electronics and Drive Systems (PEDS) 2009, 288-293.
[29]. R. Ramakumar, P. Chiradeja. Distributed generation and renewable energy systems. The 37th Intersociety Energy Conversion Engineering Conference (IECEC'02) 2002: 716-724.
[30]. E. Kamal, A. Aitouche. Fuzzy observer-based fault tolerant control against sensor faults for proton exchange membrane fuel cells. International Journal of Hydrogen Energy 2020, 45(19): 11220-11232
[31]. S. Li, A. Aitouche, H. Wang, N. Christov. Sensor fault estimation of PEM fuel cells using Takagi Sugeno fuzzy model. International Journal of Hydrogen Energy 2020, 45(19), 11267-11275.
[32]. H. Habib, F. Khoucha, A. Harrag. GA-based robust LQR controller for interleaved boost DC–DC converter improving fuel cell voltage regulation. Electric Power Systems Research 2017, 152: 438-456.
[33]. S. Somkun, C. Sirisamphanwong, S. Sukchai. A DSP-based interleaved boost DC–DC converter for fuel cell applications. international journal of hydrogen energy 2015, 40(19): 6391-6404.
[34]. A. Abbaspour, A., Khalilnejad, Z. Chen. Robust adaptive neural network control for PEM fuel cell. International Journal of Hydrogen Energy 2016, 41(44): 20385-20395.
[35]. A. Romero, L. Martínez-Salamero, H., Valderrama, O., Pallás, E. Alarcón. General purpose sliding-mode controller for bidirectional switching converters. In ISCAS'98. Proceedings of the IEEE International Symposium on Circuits and Systems (Cat. No. 98CH36187) 1998, 6: 466-469.
[36]. E. M. Navarro-López, D. Cortés, C. Castro. Design of practical sliding-mode controllers with constant switching frequency for power converters. Electric Power Systems Research 2009, 79(5), 796-802.
[37]. N. Harrabi, M. Souissi, A. Aitouche, M. Chaabane. Modeling and control of photovoltaic and fuel cell based alternative power systems. International Journal of Hydrogen Energy 2018, 43(25): 11442-11451.
[38]. S. Abdelmalek, L. Barazane, A. Larabi, M. Bettayeb. A novel scheme for current sensor faults diagnosis in the stator of a DFIG described by a TS fuzzy model. Measurement 2016, 91: 680-691.
[39]. S. Abdelmalek, A.T. Azar, D. Dib. A novel actuator fault-tolerant control strategy of DFIG-based wind turbines using Takagi-Sugeno multiple models. International Journal of Control, Automation and Systems 2018, 16(3): 1415-1424.
[40]. O. Tremblay, L. A. Dessaint. A generic fuel cell model for the simulation of fuel cell vehicles. In 2009 IEEE Vehicle Power and Propulsion Conference 20019: 1722-1729.
[41]. X. Lü, X. Miao, Y. Xue, L. Deng, M. Wang, D. Gu, X. Li. Dynamic Modeling and Fractional Order PIλD μ Control of PEM Fuel Cell. Int. J. Electrochem. Sci 2017, 12: 7518-7536.
[42]. C. H. Liu, M. Y. Hsiao. A finite time synergetic control scheme for robot manipulators. Computers & Mathematics with Applications 2012, 64(5): 1163-1169.

[43]. Z. Jiang. Design of a nonlinear power system stabilizer using synergetic control theory. Electric Power Systems Research 2009, 79(6): 855-862.
[44]. Z. Jiang, R.A. Dougal. Synergetic control of power converters for pulse current charging of advanced batteries from a fuel cell power source. IEEE Transactions on Power electronics 2004, 19(4): 1140-1150.
[45]. E. Santi, A. Monti, D. Li, K. Proddutur, R. A. Dougal. Synergetic control for DC-DC boost converter: implementation options. IEEE Transactions on industry applications 2003, 39(6): 1803-1813.
[46]. Y. Wu, Y. Huangfu, R. Ma, A. Ravey, D. Chrenko. A strong robust DC-DC converter of all-digital high-order sliding mode control for fuel cell power applications. Journal of Power Sources 2019, 413, 222-232.
[47]. A.T. Hammid, M.H.B. Sulaiman, Series division method based on PSO and FA to optimize Long-Term Hydro Generation Scheduling. Sustainable Energy Technologies and Assessments 2018, 29: 106–118.
[48]. J. Kennedy. Particle swarm optimization. Encyclopedia of machine learning 2010, 760-766.
[49]. O. Krishan and S. Suhag, Grid-independent PV system hybridization with fuel cell-battery/supercapacitor: Optimum sizing and comparative techno-economic analysis. Sustainable Energy Technologies and Assessments 2020, 37: 100625.
[50]. R. Akbarpour Ghiasi, M. Fallah, S. Lotfan, M.A. Rosen. A new approach for optimization of combined cycle system based on first level of exergy destruction splitting, Sustainable Energy Technologies and Assessments 2020, 37 100600.